Astron. Astrophys. 358, 154–168 (2000)

ASTRONOMY AND ASTROPHYSICS

Accretion disc models for AM Canum Venaticorum systems

W. El-Khoury and D. Wickramasinghe

Astrophysical Theory Centre, Department of Mathematics, Australian National University; ACT 0200, Australia
(walid,dayal@maths.anu.edu.au)

Received 16 November 1999 / Accepted 16 March 2000

Abstract. Using a model of the vertical structure of accretion discs, we calculate disc spectra across a range of system parameters for the helium-rich AM CVn cataclysmic variables, and investigate thermal instabilities in their discs.

Applying a χ^2-minimisation technique, predicted HeI and HI continuum and line profiles are compared with those observed for two such systems, AM CVn and CR Boo, to estimate several system parameters. We find:

- mean accretor masses close to, but somewhat higher than, the 0.7–$0.8M_{\odot}$ range predicted by present population synthesis studies;
- typical helium-to-hydrogen number density ratios of 10^2–10^4, consistent with a helium-degenerate donor surrounded by a helium-rich envelope; and
- mass-transfer rates of about $10^{17}\mathrm{gs}^{-1}$, which may place the systems in the region of potential disc instability.

S-curves calculated for the best-fit models are consistent with a thermally-stable disc in AM CVn, and a thermally unstable disc in CR Boo.

Key words: stars: individual: AM CVn, CR Boo – stars: novae, cataclysmic variables – stars: evolution – stars: binaries: general

1. Introduction

AM CVn systems are puzzling variable stars with hydrogen-deficient spectra and ultrashort period photometric variations in the range 1000–3000s. Only six have been observed to date. It is currently believed that they are interacting white dwarf binary (IWDB) systems (Faulkner et al. 1972) in which a low-mass white dwarf secondary of mass $M_2 \sim 0.04M_{\odot}$ fills it Roche lobe and transfers helium-rich gas to a white dwarf primary, around which a hydrogen-deficient accretion disc is formed. They are the white dwarf counterparts of the better studied neutron star binary systems, and are an interesting but little understood end-product of close binary evolution.

The original motivation behind the IWDB model was to explain a peculiar object, HZ 29 (later designated AM Canum Venaticorum, or AM CVn), following observations by Malmquist (1936) and Humason & Zwicky (1947). Greenstein & Mathews (1957) had classified HZ 29 as a DB white dwarf since it was hydrogen deficient, exhibiting only strong HeI absorption lines. Later observations suggested a quasi-stellar object (Burbidge et al. 1967) or a hot star (Wampler 1967). However, the discovery of periodic variability ($\sim$ 17min) by Smak (1967) suggested a binary system and, after discovering flickering in the high-speed photometry, Warner & Robinson (1972) suggested that AM CVn was a close binary in mass-transfer mode.

More objects with similar characteristics were identified: G61-29 (GP COM) was thought by Burbidge & Strittmatter (1971) to be an isolated white dwarf, but later photometry showed flickering activity, suggestive of a binary system (Warner 1972). PG1346+082, later designated CR Bootis, or CR Boo (Nather 1985), and V803 Cen were other objects showing similar characteristics (O'Donoghue et al. 1987). CP Eri was found by Howell et al. (1991) to be a short-period photometric variable of the AM CVn type. The latest object exhibiting AM CVn class characteristics is EC15330-1403, discovered by O'Donoghue et al. (1994).

Some class members exhibit high and low states in their optical flux, which is also strongly suggestive of a mass-transferring close binary, while others are more stable. The characteristics of this long-term variability are reminiscent of what is seen in cataclysmic variables of different sub-types – dwarf novae, nova-likes, SU UMa etc. – where a combination of thermal and tidal disc instabilities appear to play the major role in explaining the long-term variability. A similar interpretation may be possible for AM CVn systems (Warner 1995). AM CVn and EC153330 seem to be in a permanent high state, showing broad and shallow absorption lines presumably originating from a stable high mass-transfer rate $\dot{M}$ and optically-thick accretion disc – similar to nova-like variables and Z Cam systems. GP Com is the only member with a stable low state, and exhibits an emission line spectrum indicative of optically-thinner discs with lower $\dot{M}$. The other three members – CR Boo, V803 Cen and CP Eri – alternate between high and low states, with their spectra showing absorption lines in the former case, and continuous or weak emission lines in the latter case. Such behaviour is expected if $\dot{M}$ is in an intermediate range where the disc becomes thermally unstable – as in dwarf novae. Over and above the thermal instabilities, the discs in AM CVn stars are also expected to be

Send offprint requests to: W. El-Khoury

tidally-unstable by virtue of their low donor-to-accretor mass ratio $q = M_2/M_1$. Thus it has been suggested that AM CVn may be in a permanent superoutburst state exhibiting a superhump period that is slightly larger than the orbital period, making it similar to the high mass-transfer rate SU UMa variables (Osaki 1996).

In this paper we investigate the viability of a disc-instability explanation for some observed behaviour in these systems, and to constrain their parameters by modelling the spectra expected from helium-rich accretion discs and then fitting the results to observed spectra. The paper is arranged as follows. In Sect. 2 we outline the current theoretical and observational status of AM CVn and CR Boo. Sect. 3 presents the equations used to calculate the vertical structures and emergent flux of accretion discs, describing both modelling techniques and assumptions. Numerical results for disc structures and line profiles are presented in Sect. 4, together with spectral-fitting results for AM CVn and CR Boo. Finally, in Sect. 5 results are discussed, and conclusions drawn, in relation to disc instability models and independent estimates of binary masses.

2. Observations

2.1. AM CVn

Observations of AM CVn have shown the presence of multiple periodicities (Patterson et al. 1992). The 1051s period is far from stable, changing erratically from year-to-year, making it a poor candidate for the orbital period of the system. Patterson et al. (1992) suggested that this was the period of a permanent superhump due to a precessing disc, which is consistent with the low mass ratio indicated for this system. A second more coherent period at $1028.7325\text{s} \pm 0.0004$ is also seen in this system, but it sometimes changes to a period of 1011s. Harvey et al. (1998) proposed the 1028.7325s period as the actual orbital period of the system. Although the periods show complex behaviour, the disc in the system appears to be stable in the long-term, with no reports of large changes in the mean apparent magnitude. Indeed it seems that AM CVn is a system with a disc in a permanent high state, and most likely in permanent superoutburst.

In what follows we take 1028.7325s as the orbital period P_{orb}. We use as our basic source of spectral data the phase-averaged optical spectrum published by Patterson et al. (1993) – hereafter PHS – which shows characteristic features such as the shape of the continuum, line widths and the double-peaked feature of the lines. From the lack of radial velocity variations in the spectrum of AM CVn, PHS deduced that the radial velocity amplitude of the primary $K_1 < 50\text{km s}^{-1}$.

2.2. CR Bootis

CR Boo is one of the three known unstable AM CVn systems, and exhibits variations in mean apparent magnitude strongly reminiscent of those caused by thermal disc instabilities in dwarf novae.

Extensive photometric analysis – Patterson et al. (1997) and references therein – led to the current belief that its orbital period $P_{orb} = 1471$s, and that a 1490s variation is a good candidate for a superhump period which seems to stabilise at $1487.29\text{s} \pm 0.02$ after 300–600 orbits.

For our purposes, we assume $P_{orb} = 1471$s and adopt a spectrum for CR Boo in its high state kindly provided to us by J. Patterson.

3. The model

3.1. Accretion disc structure

We assume an axisymmetric disc – extending from inner radius R_{in} to outer radius R_{out} – around a central accretor, and use the geometrically-thin approximation with α-prescription for viscosity (Shakura & Sunyaev 1973) to describe the disc structure. Under these assumptions radial pressure gradients are negligible, and angular velocity is effectively the Keplerian value. In systems with extreme mass ratios, tidal effects due to the companion star will distort outer regions of the disc beyond the 3-1 resonance radius. While these distortions may be important in calculating and interpreting phase-dependent line spectra, we neglect them here as we model only phase-averaged spectra.

For mass-transfer at rate $\dot{M}$ through a thin accretion disc around a primary with negligible rotation, the effective temperature T_{eff} at disc radius R is independent of viscosity parameter α and given by (Frank et al. 1992)

$$T_{eff}^4 = \frac{3}{8\pi\sigma}\left(\frac{GM_1\dot{M}}{R^3}\right)\left\{1-\left(\frac{R_1}{R}\right)^{1/2}\right\}, \quad (1)$$

where σ and G are the Stefan-Boltzmann and gravitational constants respectively. Note that the radius R_1 of the white dwarf may be related to its mass M_1 and the Chandrasekhar limiting mass M_{ch} by (Nauenberg 1972)

$$R_1 = 7.79\times10^8\left\{\left(\frac{M_1}{M_{ch}}\right)^{-2/3}-\left(\frac{M_1}{M_{ch}}\right)^{2/3}\right\}^{1/2}\text{cm}, \quad (2)$$

and that T_{eff} may be expressed as

$$T_{eff} = 7.837\ \times\ 10^4\left(\frac{M_1}{M_\odot}\right)^{1/2}\left(\frac{\dot{M}}{10^{17}}\right)^{1/4} \times\ \left(\frac{R}{R_1}\right)^{-7/8}\left\{\left(\frac{R}{R_1}\right)^{1/2}-1\right\}^{1/4}\text{K}, \quad (3)$$

where $\dot{M}$ is measured in gs^{-1} and we have used a simplified version of (2)

$$\frac{R_1}{R_\odot} = 0.013\left(\frac{M_1}{M_\odot}\right)^{-1/3}. \quad (4)$$

Typically for AM CVn stars, T_{eff} falls from $T_{in} = 5\times10^4$K to $T_{out} = 10^4$ K as R increases from R_{in} to R_{out}.

We calculate the radial and vertical structure of an accretion disc – ignoring convection – as follows. We first divide the disc into a number of elemental rings of width δR: the choice of this

number, as well as of R_{in} and R_{out}, will be discussed below. For each ring, radiative transfer in the vertical direction z is treated in the two-stream grey approximation, using a formulation similar to that in Wehrse et al. (1994) – see also Shaviv & Wehrse (1986). They assume the two streams of radiation to travel normal to the disc, but we assume they travel at angle $\theta = \cos^{-1}(1/\sqrt{3})$ to the normal, which means we may use conventional Gaussian quadrature to approximate the flux integral. We stress that variations in disc structures between the two formulations are minimal.

The frequency-integrated flux, F, and mean intensity, J, are defined in terms of the frequency-integrated intensity I by

$$F = \int_{-1}^{1} I\mu d\mu, \tag{5}$$

$$J = \frac{1}{2}\int_{-1}^{1} I d\mu, \tag{6}$$

where $\mu = \cos\theta$. Using n-point Gaussian quadrature with weighting-factors a_i and corresponding outgoing and incoming intensities I_i^+ and I_i^- respectively, these expressions become

$$F = 2\pi \sum_{i=1}^{n} a_i \{\mu_i I_i^+ - \mu_i I_i^-\}, \tag{7}$$

$$J = \frac{1}{2} \sum_{i=1}^{n} a_i \{I_i^+ - I_i^-\}. \tag{8}$$

For the two-stream approximation $n = 1$, $a_1 = 1$ and $\mu_1 = 1/\sqrt{3}$, in which case

$$F = 2\pi\mu_1 (I^+ - I^-), \tag{9}$$

$$J = \frac{1}{2}(I^+ + I^-). \tag{10}$$

With no irradiation and assuming the LTE approximation, the model equations for an elemental ring at disc radius R with local gas density ρ become

$$\frac{dF}{dz} = 4\pi\kappa_R (\frac{\sigma T^4}{\pi} - J), \tag{11}$$

$$\frac{dJ}{dz} = -\frac{\chi F}{4\pi\mu_1^2}, \tag{12}$$

$$\frac{dP_g}{dz} = -\Omega_K^2 z\rho + \frac{\chi}{c}F, \tag{13}$$

$$4\pi\kappa_R (\frac{\sigma T^4}{\pi} - J) = \frac{3}{2}\alpha\Omega_K P_g, \tag{14}$$

which give the grey flux F, mean intensity J, gas pressure P_g and temperature T as functions of z: κ_R and χ are Rosseland mean of absorption and extinction coefficients respectively, $\rho = \rho(T, P_g)$ assuming an ideal gas, and Ω_K is the angular velocity at disc radius R given by

$$\Omega_K = \sqrt{\frac{GM_1}{R^3}} = 0.423 \left(\frac{M_1}{M_\odot}\right)^{1/2} \left(\frac{R}{R_1}\right)^{-3/2} \mathrm{s}^{-1}, \tag{15}$$

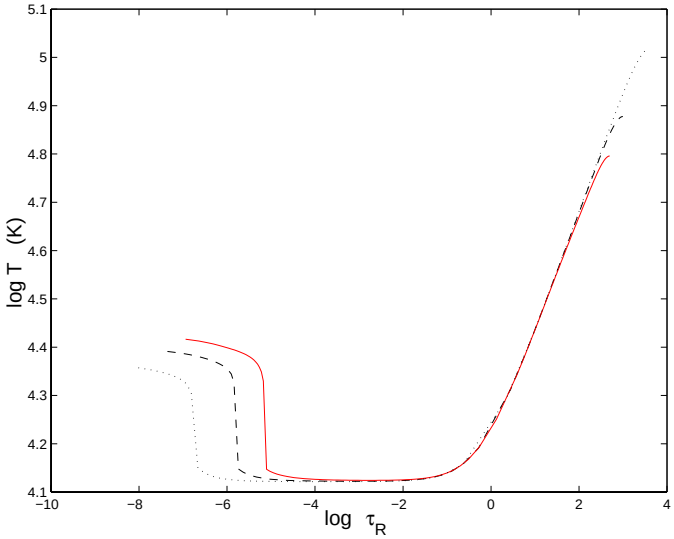

Fig. 1. Vertical temperature distribution at disc radius $R = 7.4\times10^9$cm with $\log \dot{M}(\mathrm{gs}^{-1}) = 17.0$, $M_1 = 1M_\odot$, $\Gamma = 10^3$ and $T_{eff} = 1.5 \times 10^4$K. Dotted line: $\alpha = 0.05$. Dashed line: $\alpha = 0.3$. Solid line: $\alpha = 1.0$

the latter form assuming the white dwarf mass-radius relationship (4).

The above constitute a closed algebraic-differential equation system for a *boundary-value* problem with eigenvalue z_0, the semi-thickness of the disc. Boundary conditions at the surface of the disc, $z = z_0$, are

$$F(z_0) = \sigma T_{eff}^4,$$

$$J(z_0) = \frac{\sigma T_{eff}^4}{4\pi\mu_1},$$

$$P_g(z_0) = P_0,$$

with P_0 chosen such that the line formation region is fully within the calculated structure (e.g., $\log P_0 \sim -3$) and $T(z_0)$ is determined via the energy-balance equation (14). From symmetry, the boundary condition at the disc mid-plane, $z = 0$, is

$$F(0) = 0. \tag{16}$$

The eigenvalue z_0 is calculated iteratively until the model converges to the solution satisfying (16), which is the solution for the vertical structure of the accretion disc ring at radius R. The adaptive finite-difference code FORTRAN DASSL (Brenan et al. 1989) is used to solve the equations. Although DASSL is presented as an *initial-value* algebraic-differential equation solver, we treat the boundary conditions at z_0 as initial values, and then iteratively solve for the central boundary condition at $z = 0$ using Newton's method.

We specify $\alpha = 0.3$ as a typical value for a high-state viscosity parameter. But it is important to subject this assumption to sensitivity analysis because, while T_{eff} is independent of α, the energy equation (14) does incorporate α. Fig. 1 shows the temperature structure for an accretion disc ring at $R = 7.4\times10^9$cm for the three values $\alpha = 0.05$, 0.3 and 1.0. Clearly, while disc coronal structures are sensitive to α, the line formation regions

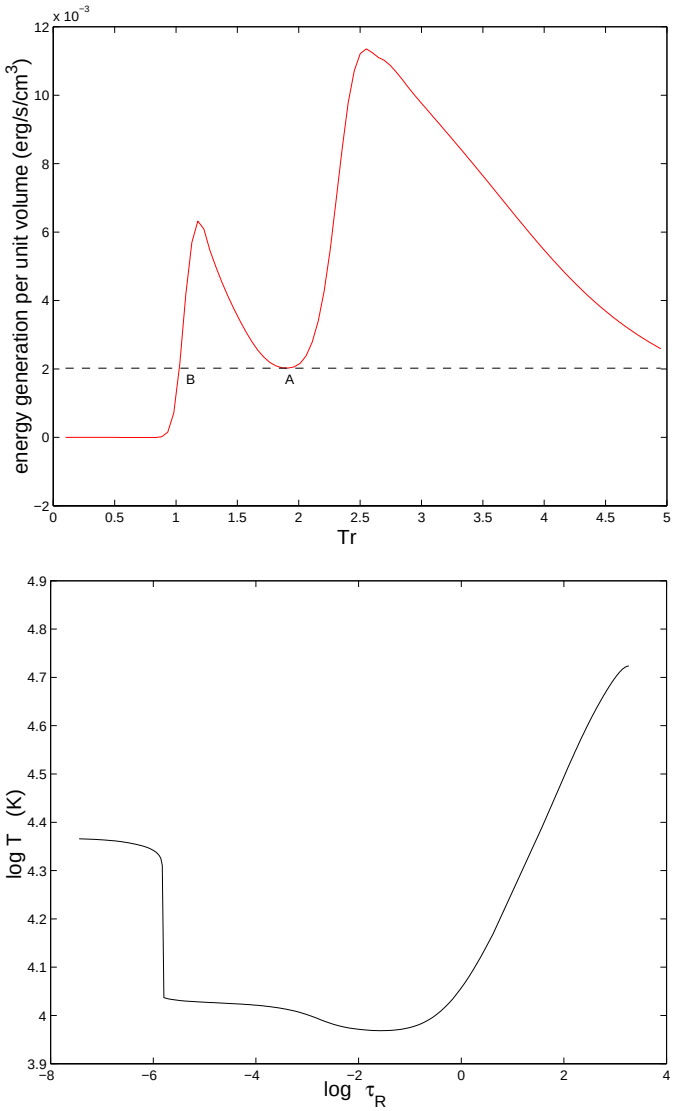

Fig. 2. Model solutions for a disc ring with $T_{eff} = 1.1 \times 10^4$K at $R = 1.2 \times 10^{10}$cm with $\log \dot{M}(\mathrm{gs}^{-1}) = 17.0$, $M_1 = 1M_\odot$, $\Gamma = 10^3$ and $i = 15^o$. Top: the right-hand (dashed line) and left-hand (solid line) sides of (14) versus $Tr = T/T_{eff}$ Bottom: the vertical temperature structure.

in the photosphere – and hence the model spectra – are relatively insensitive. Therefore we are justified in using $\alpha = 0.3$ in our investigations.

It is well known – e.g., Adam et al. (1988) – that the energy equation sometimes yields more than one solution for temperature at a given pressure. Typically there are two thermally-stable solutions, one of which starts with a hot corona at low optical depths but matches, with increasing optical depth, onto a cooler disc structure: the other is a cold solution at all optical depths. The top panel of Fig. 2 shows a typical solution for (14): the dashed straight line represents the right-hand side of the equation, and the solid line the left-hand side – the two peaks are due to HeI and HeII ground-state jumps. The intersection of these two lines is the solution to (14) so, in general, there are four solutions, two of which are unstable – those on negative-sloping portions of the solid line. The other two stable solutions – termed here "hot" and "cold" – are on positive-sloping portions of the solid line. There is a transition from a hot to a cold solution at the tangent point A, where (14) becomes too difficult to solve numerically, causing a jump to the cold solution at B. This transition is also evident as a discontinuity in the temperature distribution shown in the bottom panel of Fig. 2, but it occurs at much shallower optical depths than the line formation region and so does not influence the emitted spectrum.

3.2. Line and continuum flux calculations

The disc structure calculations described above yield P, ρ, T and J as functions of R and z. In order to estimate line and continuum fluxes, the disc is divided into elements bounded by $R, R + \delta R$ and $\phi, \phi + \delta\phi$ where ϕ is the rotational azimuth measured from the projected line-of-sight on the disc. Radiation at a given frequency ν and inclination angle i in the observer's frame comes from Doppler-shifted frequency $\nu_d(R, \phi)$ in the rest frame of each disc element where, if c is the velocity of light

$$\nu_d(R, \phi) = \frac{\nu}{(1 - v_{proj}/c)}, \tag{17}$$

$$v_{proj} = R\Omega_K(R) \sin i \sin \phi. \tag{18}$$

Monochromatic line and continuum opacities $\kappa_{\nu_d}(R, z)$ are then calculated, and the full plane-parallel atmosphere radiative transfer equation is solved in the frame of the disc element. This yields the emergent intensity $I_{\nu_d}(\mu, R, z_0)$ at the surface $z = z_0$ of each element (R, ϕ) of the disc, where $\mu = \cos i$. The flux radiated from the surface of the disc is then calculated as

$$F_\nu = \int_R \int_\phi I_{\nu_d}(\mu, R, z_0) \mu R d\phi dR, \tag{19}$$

and the apparent monochromatic flux which is observed

$$f_\nu = \frac{F_\nu}{d^2}, \tag{20}$$

where d is the distance of the system from the Earth. These results are used to calculate absolute visual magnitudes for the model disc in order to estimate d, as well as mean colours B-V and U-B for direct comparison with observation.

In calculating the monochromatic and Rosseland opacities, we have included bound-free and free-free continuum opacities due to hydrogen, HeI and HeII but have neglected metals. Given the uncertainties in the treatment of viscosity along with the LTE approximation, this assumption is expected to be of secondary importance in determining details of the vertical structure. Optical spectra are calculated including the HeI lines shown in Table 1 and the H_β line $\lambda 4861$, allowing for Stark and thermal Doppler-broadening. Although most of the strong HeI lines have been included, some lines near series limits have been omitted because of inadequate line data. For this reason, some discrepancies in line modelling could arise with blended lines such as $\lambda 3867$ and $\lambda 3889$.

Table 1. HeI lines included in the model

3820	2p-6d triplet
3889	2s-3p triplet
3965	2s-4p singlet
4026	2p-5d triplet
4121	2p-5s triplet
4144	2p-6d singlet
4169	2p-6s singlet
4388	2p-5d singlet
4472	2p-4d triplet
4713	2p-4s triplet
4922	2p-4d singlet
5016	2s-3p singlet
5048	2p-4s singlet
5876	2p-3d triplet

We use a χ^2-minimisation technique to fit observed and modelled spectra, seeking the minimum helium-to-hydrogen number density ratio Γ which gives negligible H_β line compared with the HeI lines, and which also reproduces the general shape of the observed spectrum. The fitting is conducted in that part of the spectrum containing most of the above lines, with a considerable part of the continuum also included so as to properly fit the continuum slope.

The best part of the spectrum for χ^2-minimisation fitting turns-out to be $4350 \leq \lambda(\text{Å}) \leq 5800$ for AM CVn, and $4350 \leq \lambda(\text{Å}) \leq 5100$ for CR Boo. In the latter case, this excludes the region around $\lambda 5170$, where Patterson et al. (1997) note the likelihood of a Fe/Mg-blend feature: use of this region would therefore require an extension of the model to include metal opacities. Interestingly, inclusion of the interval $\lambda < 4350$ Å in the fitting routine yields, for both AM CVn and CR Boo, either no solution or the physically unrealistic one $M_1 > M_{ch}$: this may be because of insufficient lines in our model spectra or calibration difficulties with the observed data. To examine the possibility that a blue spectral contribution from the primary could influence the fitting, we included in some model runs a contribution to the spectrum from a black-body at the same T_{eff} as the accretor: we found the contribution to be typically less than 10% and therefore negligible.

3.3. Parameters for the secondary

The secondaries in helium-rich cataclysmic variables could be degenerate helium white dwarfs (Faulkner et al. 1972), non-degenerate helium stars (Savonije et al. 1986) or helium-mantle stars with CO cores (Tutukov & Yungelson 1996 – hereafter TY96). Although predicted birth rates of these three types differ only by factors of 2–10, current estimates based on binary evolution models suggest that the degenerate category will predominate in magnitude-limited samples: predicted numbers are typically higher by factors of 10^3 compared to systems with non-degenerate helium stars, and typically 10^5 compared to systems with helium mantle stars (TY96). The most promising model for AM CVn systems appears therefore to be an IWDB model where the donor is a low-mass helium-degenerate white dwarf. However for the sake of completeness, we also consider the possibility that the donor may be a semi-degenerate helium star – see Warner (1995) for a review and discussion.

Assuming a semi-degenerate donor, its mass-radius relationship is (Savonije et al. 1986)

$$\frac{R_2}{R_\odot} = 0.029 \left(\frac{M_2}{M_\odot}\right)^{-0.19}, \tag{21}$$

Eliminating binary separation a between the expression for orbital period

$$P_{orb} = 2\pi \left\{\frac{a^3 q}{GM_2(1+q)}\right\}^{1/2}, \tag{22}$$

and the approximate expression when $q < 0.8$ for the donor's Roche lobe radius (Paczyński 1971)

$$R_{L2} = 0.462a \left(\frac{q}{1+q}\right)^{1/3}, \tag{23}$$

we find

$$R_{2L}^3 = \frac{(0.462)^3}{4\pi^2} GM_2 P_{orb}^2. \tag{24}$$

Therefore, in the mass-transfer situation when $R_2 = R_{L2}$, we find from (24) and (21) that

$$\begin{aligned} \frac{M_2}{M_\odot} &= \left(\frac{0.029 R_\odot}{0.462 M_\odot^3}\right)^{1.91} \left(\frac{4\pi^2}{GP_{orb}^2}\right)^{0.64} \\ &= 629.0 P_{orb}^{-1.27}(\text{s}), \end{aligned} \tag{25}$$

which gives $M_2 = 0.0921 M_\odot$ and $M_2 = 0.058 M_\odot$ for AM CVn and CR Boo respectively.

On the other hand, if we assume a fully-degenerate secondary, then as previously noted

$$\frac{R_2}{R_\odot} = 0.013 \left(\frac{M_2}{M_\odot}\right)^{-1/3}, \tag{26}$$

and, following the same procedure as above, we find that $M_2 = 0.046 M_\odot$ for AM CVn and $M_2 = 0.032 M_\odot$ for CR Boo. In our models we assume fully-degenerate mass values for the donor but discuss, towards the end of the paper, the ramifications of varying this assumption.

3.4. Range limits for the accretion disc

We have assumed in all our calculations that the disc extends to the surface of the white dwarf accretor, i.e., $R_{in} = R_1$. As we adopt M_1 as the main free-parameter in the model we find R_1, and hence R_{out}, from (2), i.e.,

$$R_{out} = 7.79 \times 10^8 \left\{\left(\frac{M_1}{M_{ch}}\right)^{-2/3} - \left(\frac{M_1}{M_{ch}}\right)^{2/3}\right\}^{1/2}. \tag{27}$$

An *upper limit* for R_{out} is clearly the accretor's Roche lobe radius R_{L1} which (Eggleton 1983) is well-approximated for all q by

$$R_{L1} = \frac{0.49q^{-2/3}a}{0.6q^{-2/3} + \ln(1+q^{-1/3})} \quad (28)$$

or, using (22), by

$$R_{L1} = \frac{0.49q^{-1}}{0.6q^{-2/3} + \ln(1+q^{-1/3})} \times \left\{\frac{GM_2(1+q)}{4\pi^2}P_{orb}^2\right\}^{1/3}. \quad (29)$$

We have estimates of M_2 from above and know P_{orb} from observations so, with M_1 as the main free-parameter, we may find R_{L1} and hence an upper limit for R_{out}. More refined estimates of R_{out} are discussed next in the context of setting a range grid for solving the disc-structure equations.

3.5. Setting the model grid

Given viscosity parameter α, disc structure – and thus the emergent spectrum – may be calculated once R_{out}, $\dot{M}$, M_1, Γ and i are specified. To do this, for a given value of R_{out}, we form the four parameter grid: $0.5 \leq (M_1/M_\odot) \leq 1.4$, $2 \leq \log\Gamma \leq 4$, $16.5 \leq \log\dot{M}(\mathrm{gs}^{-1}) \leq 18.0$ and $15^o \leq i \leq 75^o$. Then, aided by the χ^2-minimisation technique, we use this grid to seek those parameters generating model spectra which best fit the observed spectra of AM CVn and CR Boo.

Note that R_{out} is not used as a grid parameter: this is because the concomitant increase in computing time is not warranted by increased precision in comparison with simple models of disc size. The above analysis showing that $R_{out} \leq R_{L1}$ is one such simple model, while the *tidal radius* concept (Frank et al. 1992) suggesting that $R_{out} = 0.9R_{L1}$ is a related one. Yet another arises by considering streamlines at the outer edge of a close binary accretion disc – where disc pressure and viscosity are very small – as simple periodic orbits in the restricted three-body problem. Paczyński (1977) found in these circumstances that the maximum radius of the last stable orbit

$$R_{st} = r_{max}a \quad (30)$$

for tabulated $r_{max} = r_{max}(q)$. For all q corresponding to stellar masses of interest here – i.e., $0.5 \leq (M_1/M_\odot) \leq 1.3$ and $0.03 \leq (M_2/M_\odot) \leq 0.1$ – the tables show that $r_{max} = 0.48$ to within 1%. So, using (28), a *lower limit* for R_{out} is

$$R_{st} = 0.98\{0.6 + q^{2/3}\ln(1+q^{-1/3})\}R_{L1}, \quad (31)$$

in which case, for the q values of interest here, $0.71 \leq (R_{st}/R_{L1}) \leq 0.92$. Hence $R_{st} \leq R_{out} \leq R_{L1}$ and accordingly, when using the model, we construct two range grids; one with $R_{out} = R_{L1}$ and the other with $R_{out} = R_{st}$. While best fits from these two grids are not greatly different, indications are that R_{out} is in fact closer to R_{L1}, and that is the value we use to present spectral fits.

Note also that, because R_{L1} from (28) is not very sensitive to changes in q for typical AM CVn system configurations and hence – from (31) – neither is R_{st}, our model results for AM CVn systems are relatively insensitive to q. In particular, changing from fully to semi-degenerate values for M_2 does not greatly change predicted disc spectra.

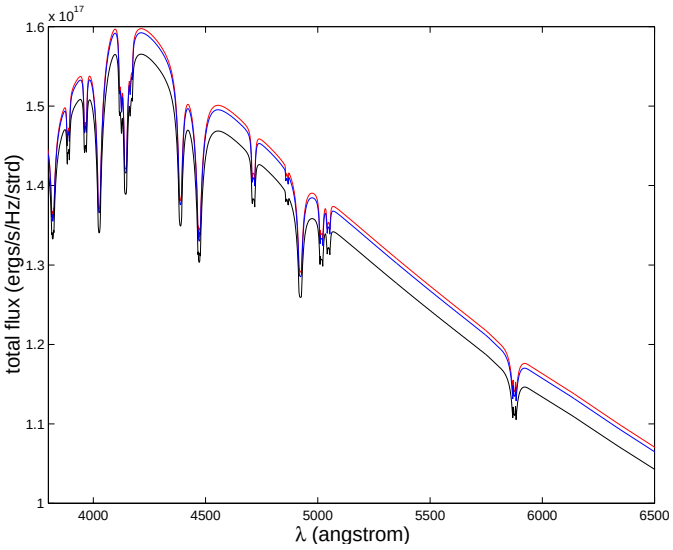

Fig. 3. Disc spectra with $R_{out} = 1.3\times10^{10}$cm, $\log\dot{M}(\mathrm{gs}^{-1}) = 16.5$, $M_1 = 1M_\odot$, $\Gamma = 10^3$ and $i = 15^o$. Upper to lower: 30, 20 and 10 elemental rings

As a practical compromise between model accuracy and computing time we divide the disc into 10 equally-spaced elemental rings. To demonstrate the reasonableness of this compromise, Fig. 3 shows spectra for an accretion disc which have been calculated with 10, 20 and 30 elemental rings: the difference in half-maximum line widths for $\lambda4471$ between a 10-ring and 30-ring disc is less than 0.1%.

As a further measure to economise on computing resources, all discs are initially constructed with $R_{out} = 1.3\times10^{10}$cm – larger than any disc anticipated for either AM CVn or CR Boo. Then, for each M_1 point in the grid, this large disc is cut-down in size to the appropriate $R_{out} = R_{st}$ or R_{L1}, both of which depend on q. In other words, for given $\dot{M}$, M_1, Γ and i, we use the same $R_{out} = 1.3\times10^{10}$cm disc to construct discs with various $R_{out} \leq 1.3\times10^{10}$cm.

4. Results

To help understand the χ^2-minimisation fitting results presented later in this section, we first examine whether the $\nu^{1/3}$ spectrum common in accretion discs – e.g., Wade 1984 – is expected in AM CVn systems. This is followed by an investigation of the influence of parameters R_{out}, $\dot{M}$, M_1, Γ and i on the continuum energy distribution and line profiles for radiation emitted by accretion discs.

4.1. The general shape of the spectrum

In an optically-thick accretion disc, one can approximate the flux from an elemental ring at radius R by that of a black body with effective temperature given by (1), and so – see Frank et al. 1992 – the *total disc* flux is

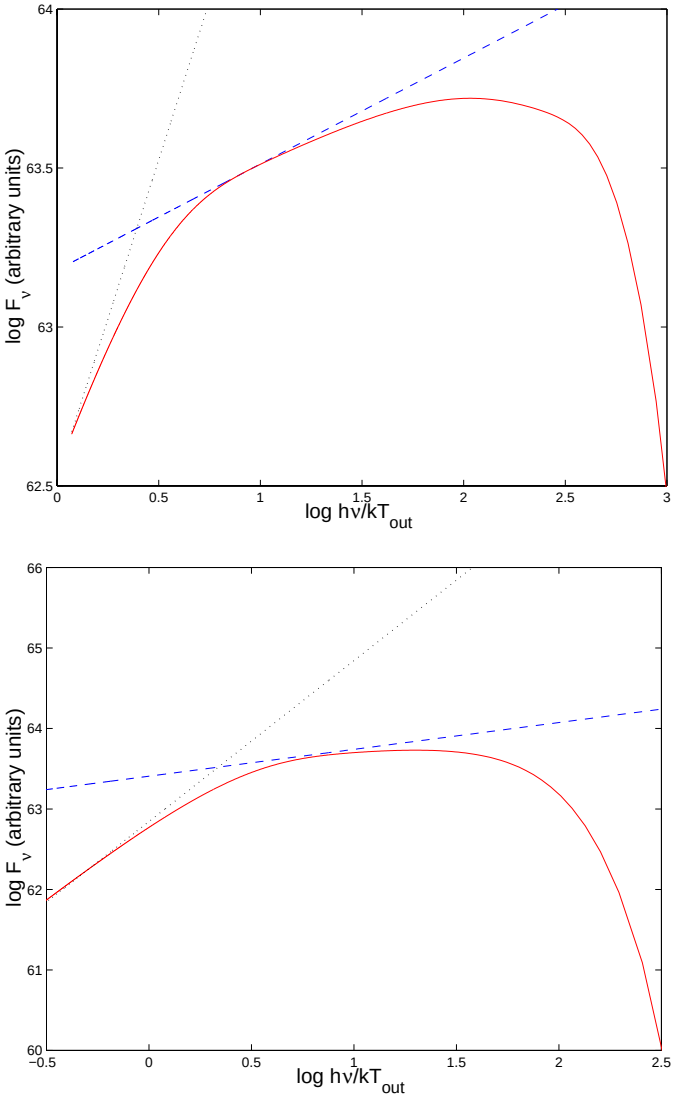

Fig. 4. The continuum flux F_ν of a disc radiating as a black body (solid line) with $\log \dot{M}(\mathrm{gs}^{-1}) = 17.0$, $M_1 = 1M_\odot$, $\Gamma = 10^3$ and $i = 15^o$. The dashed line is $\propto \nu^{1/3}$ and the dotted line is $\propto \nu^2$. Top: $R_{out} = 10^{12}$cm. Bottom: $R_{out} = 10^{11}$cm.

$$F_\nu = \frac{4\pi h\nu^3 \cos i}{c^2} \int_{R_1}^{R_{out}} \frac{RdR}{\exp(h\nu/kT_{eff}) - 1}, \qquad (32)$$

where h is Planck's constant. Note that the flux is independent of α, which is characteristic of optically-thick discs in a steady-state. For small frequencies – $\nu \ll kT_{out}/h$ – we have the Rayleigh-Jeans behaviour $F_\nu \propto \nu^2$, while for large frequencies – $\nu \gg kT_{out}/h$ – we have the Wien form $F_\nu \propto \nu^2 \exp(-h\nu/kT_{eff})$. Moreover if $R_{out} \gg R_1$, the limits of the integral in (32) tend to 0 and ∞, and (1) tends to

$$T_{eff}^4 = \frac{3}{8\pi\sigma}\left(\frac{GM_1\dot{M}}{R^3}\right), \qquad (33)$$

in which case $F_\nu \propto \nu^{1/3}$.

Fig. 4 shows the emergent flux from accretion discs of different size which are emitting as black bodies; spectra proportional to ν^2 and $\nu^{1/3}$ are superimposed. That part of the spectrum proportional to $\nu^{1/3}$ is clearly not very extensive, and it becomes smaller as R_{out} decreases from 10^{12} to 10^{11} cm – i.e., as T_{out} increases. For this reason we do not expect the model spectra to have the $\nu^{1/3}$ form for $R_{out} \sim 10^9$cm, which is a typical AM CVn accretion disc size.

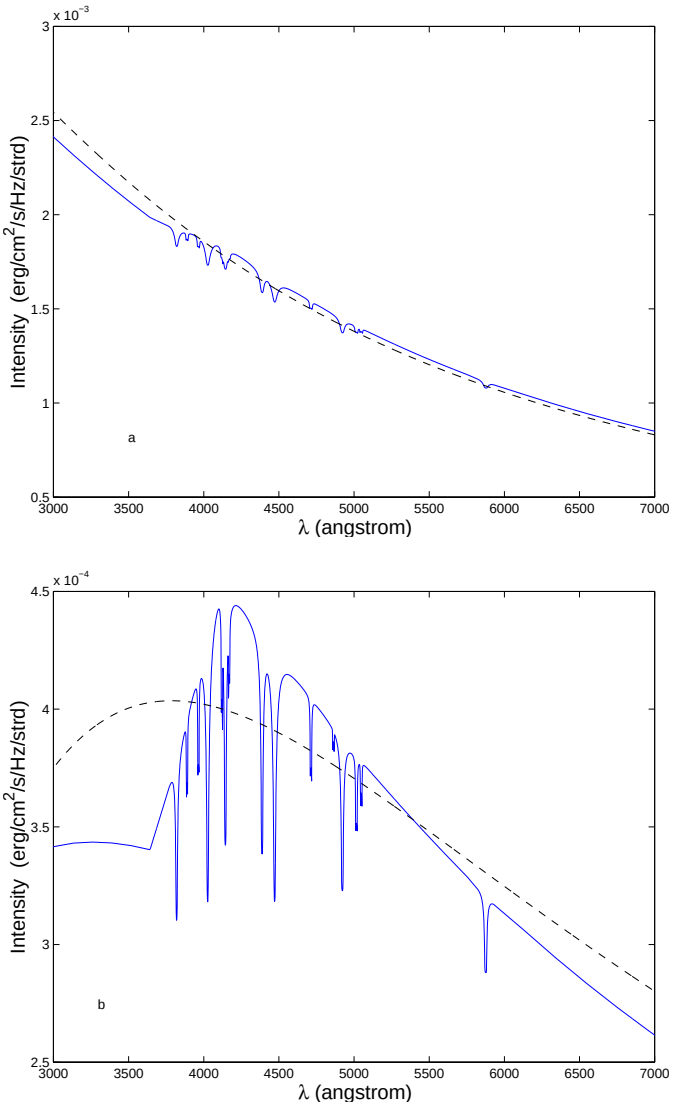

Fig. 5a and b. Optical spectra (solid line) from the outer ring in accretion discs with $\log \dot{M}(\mathrm{gs}^{-1}) = 17.0$, $M_1 = 1M_\odot$, $\Gamma = 10^3$ and $i = 15^o$, superimposed on black-body spectra of the same effective temperature (dashed line). Top: ring at $R = 2.9 \times 10^9$cm, $T_{eff} = 2.85 \times 10^4$K. Bottom: ring at $R = 8.6 \times 10^9$cm, $T_{eff} = 1.35 \times 10^4$K.

We would also expect departures from the black-body spectrum to be more evident in *disc regions* where the grey conditions assumed in the model clearly do not hold. For example, Fig. 5a shows the optical spectrum of a ring at 2.9×10^9cm superimposed on a black-body spectrum of the same effective temperature as the ring, $T_{eff} = 2.85 \times 10^4$K; the fit between the two is good. However, Fig. 5b shows the spectrum for a ring at $R = 8.6 \times 10^9$cm where $T_{eff} = 1.35 \times 10^4$K, and it is clear that the corresponding black-body spectrum does not match the

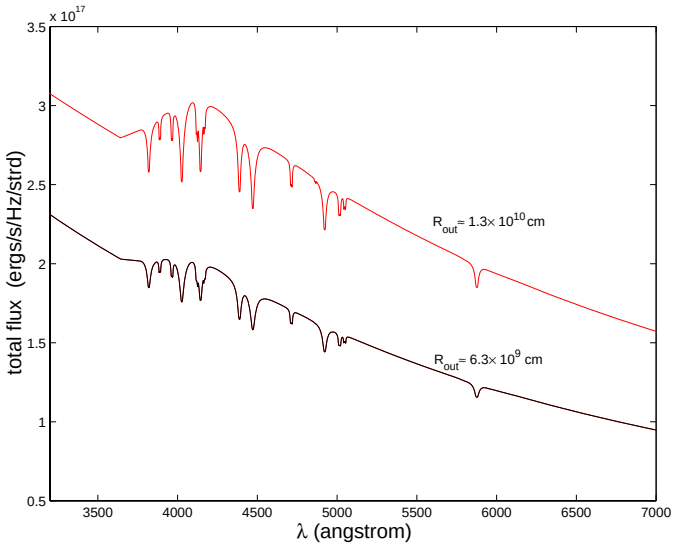

Fig. 6. Optical spectra for two accretion discs with $\log \dot{M}(\mathrm{gs}^{-1}) = 17.0$, $M_1 = 1M_\odot$, $\Gamma = 10^3$ and $i = 15^o$. Upper: $R_{out} = 1.3 \times 10^{10}$cm. Lower: $R_{out} = 6.3 \times 10^9$cm.

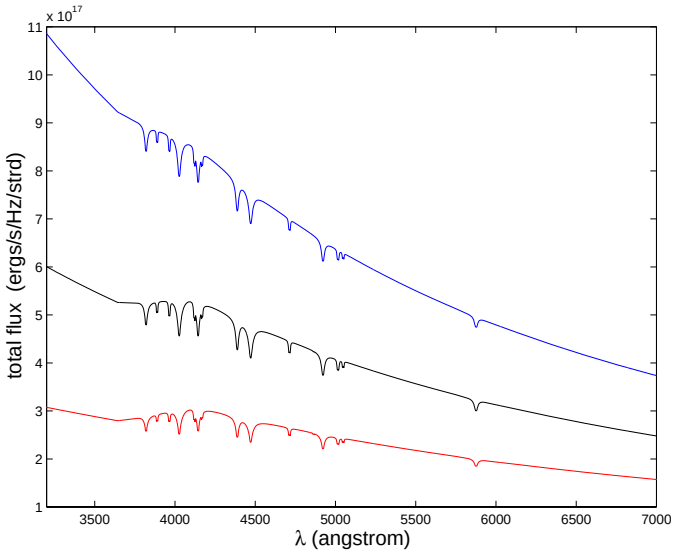

Fig. 7. Optical spectra for an accretion disc with $R_{out} = 1.3 \times 10^{10}$cm, $M_1 = 1M_\odot$, $\Gamma = 10^3$ and $i = 15^o$. Upper to lower: $\log \dot{M}(\mathrm{gs}^{-1}) = 18.0,\ 17.5and17.0$.

model spectrum nearly as well. This is not surprising considering the non-grey nature of the opacities – e.g., HeI continuum jumps – in the cooler region.

4.2. Effects of disc parameters on the spectra

4.2.1. Disc size R_{out}

Fig. 6 shows spectra for discs with $R_{out} = 1.3 \times 10^{10}$cm and 6.3×10^9cm. In general, if all other parameters are held constant, line profiles become deeper and narrower with increasing disc radius. This is expected, because contributions to spectral lines come predominantly from the cooler outer disc rings – with their larger surface area – where lines are less affected by Stark-broadening as well as Doppler-broadening, and thus have sharper features.

4.2.2. Mass-transfer rate $\dot{M}$

Fig. 7 shows spectra for an accretion disc at three different mass-transfer rates $\log \dot{M}(\mathrm{gs}^{-1}) = 17, 17.5and18$. The increase in T_{eff} with increasing $\dot{M}$ steepens the slope of the blue continuum and deepens the lines while T_{eff} is less than the peak ionisation temperature for HeI. At higher values of $\dot{M}$, HeI is fully-ionised and this effect is reversed.

4.2.3. Accretor mass M_1

Fig. 8 shows that, as expected from (1), the effect of increasing gravity as M_1 increases is similar to that of $\dot{M}$ noted above; i.e., the continuum slope and line depths increase with increasing M_1. But, as $M_1 \propto R_1^{-3}$, the M_1-effect is even more pronounced because the $(R_1/R)^{1/2}$ term in (1) – although small – decreases as M_1 increases. In addition, both pressure and rotational line broadening (for $i \neq 0^o$) increase with M_1.

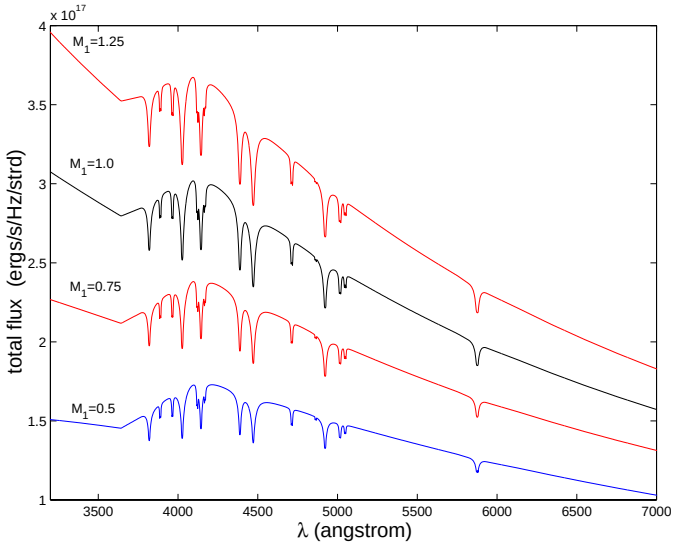

Fig. 8. Optical spectra for an accretion disc with $R_{out} = 1.3 \times 10^{10}$cm, $\log \dot{M}(\mathrm{gs}^{-1}) = 17.0$, $i = 15^o$. Upper to lower: $(M_1/M_\odot) = 1.25,\ 1.0,\ 0.75and0.5$.

4.2.4. Hydrogen-to-helium number ratio Γ

Although Γ is clearly important in determining the strengths and shapes of spectral lines (indeed we use it as a key fitting-parameter), its effects may be masked by other factors. For instance, a weak but not negligible H_β line may not be observed in an inclined disc because of the $\sin i$-dependence of Doppler-broadening. Again, a particular Γ might give a significant H_β contribution from the middle of a disc but not, because of the different fractional ionisations, from the inner (hotter) and outer (colder) regions. An absence of observed H_β may then be due to either lack of hydrogen, or masking of lines emitted from the middle by the continuum from elsewhere in the disc.

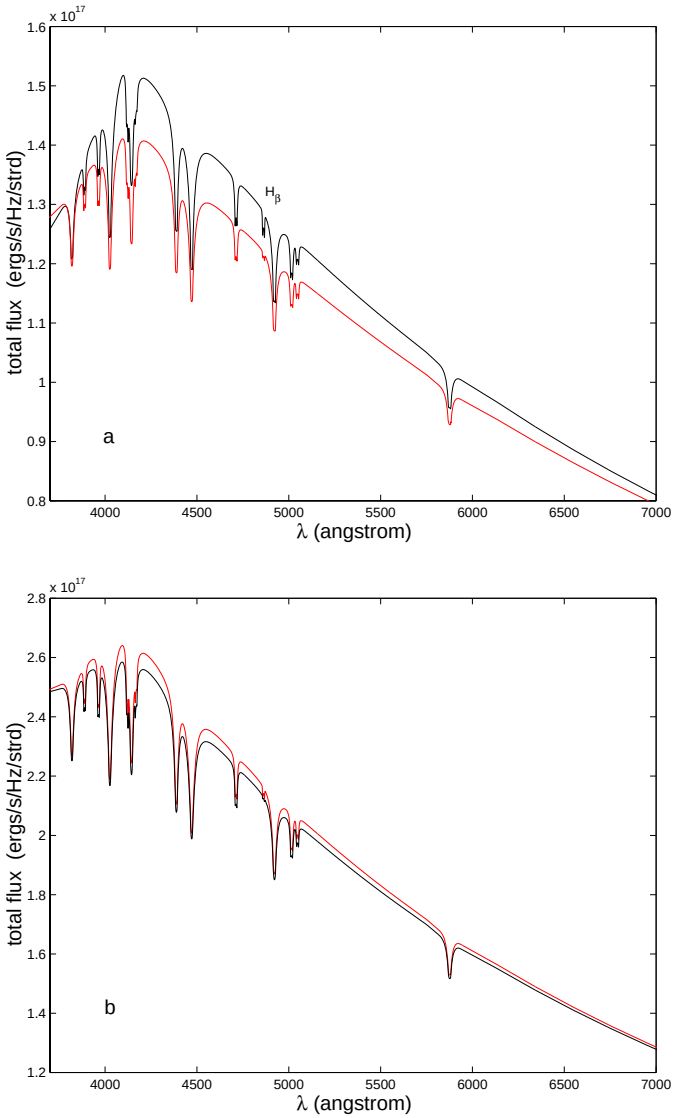

Fig. 9a and b. Optical spectra for an accretion disc with $R_{out} = 8.6 \times 10^9$cm, $M_1 = 1M_\odot$ and $i = 15^o$. Panel **a**: $\log \dot{M}(\mathrm{gs}^{-1}) = 16.5$, with (upper) $\Gamma = 10^2$ and (lower) $\Gamma = 10^3$. Panel **b**: $\log \dot{M}(\mathrm{gs}^{-1}) = 17.0$, with (upper) $\Gamma = 10^2$ and (lower) $\Gamma = 10^3$.

The spectral influence of Γ is strongly-dependent on T_{eff} – and hence $\dot{M}$ – as is shown in Fig. 9. Fig. 9a shows spectra from two discs differing only in that $\Gamma = 10^2$ for the upper one and 10^3 for the lower: the H_β line, clearly visible with $\Gamma = 10^2$, almost disappears for $\Gamma = 10^3$. The disc configuration for Fig. 9b is similar except for a higher mass-transfer rate: with almost total hydrogen ionisation, the H_β line disappears even when $\Gamma = 10^2$.

4.2.5. Inclination angle i

Fig. 10 shows the effect of varying inclination angle on the emergent spectrum from an accretion disc. Because of the $\sin i$-dependence of Doppler effects:

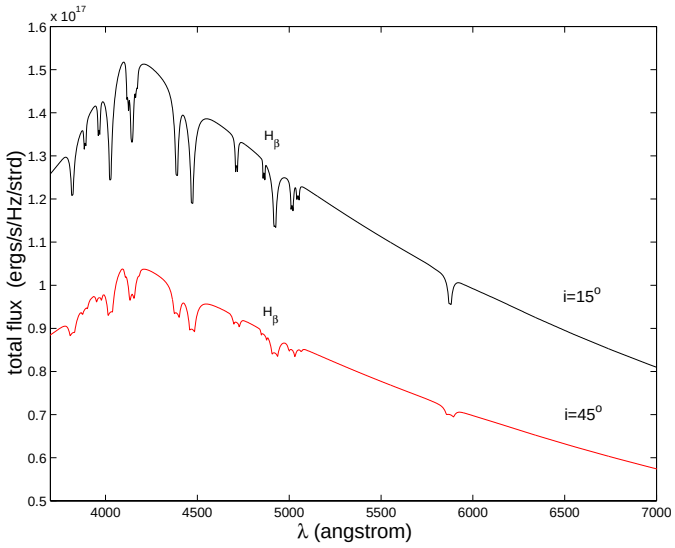

Fig. 10. Optical spectra for an accretion disc with $R_{out} = 1.3 \times 10^{10}$cm, $\log \dot{M}(\mathrm{gs}^{-1}) = 16.5$, $M_1 = 1M_\odot$ and $\Gamma = 10^2$. Upper: $i = 15^o$. Lower: $i = 45^o$.

– the double-peaked feature of Doppler-broadened lines is clear for $i = 45^o$ but not for $i = 15^o$, and
– the H_β line for $i = 45^o$ is relatively weak compared to $i = 15^o$.

The enhanced total flux from the disc when $i = 15^o$ arises primarily because the projected surface area of the disc seen by the observer depends on $\cos i$.

4.3. Models of best fit for AM CVn

In Figs. 11 and 12 we present confidence contours from the χ^2-fitting for AM CVn with $R_{out} = R_{st}$ and R_{L1}. Best-fit parameters, with one standard deviation error estimates, are:

– $R_{out} = R_{st}$ gives $M_1 = 0.77M_\odot \pm 0.11$, $\log \dot{M}(\mathrm{gs}^{-1}) = 17.0 \pm 0.2$, $i = 46.0^o \pm 2.6$ and $\log \Gamma > 2.5$; while
– $R_{out} = R_{L1}$ gives $M_1 = 0.90M_\odot \pm 0.2$, $\log \dot{M}(\mathrm{gs}^{-1}) = 17.1 \pm 0.2$, $i = 43.7^o \pm 3.5$ and $\log \Gamma > 2.4$.

Averaged values are $M_1 = 0.84M_\odot$, $\log(\dot{M}(\mathrm{gs}^{-1}) = 17.0$ and $i = 44.9^o$. The value for M_1 is near the $0.65M_\odot$ peak value of the distribution of primary masses predicted for AM CVn systems in TY96.

The difference in fit between the two cases is not great, although an increase in M_1 with increasing R_{out} is evident. This may be explained by two competing effects noted earlier:

– the deepening and narrowing of line profiles with increasing R_{out}, and
– the increase in both pressure and rotational line broadening (for $i \neq 0^o$) with increasing M_1.

Therefore, when fitting a particular observed line profile, a larger R_{out} needs an increase in M_1 to compensate for the narrow-line contribution from the outer disc regions. So more precise estimates of M_1 – and to a lesser extent the other disc parameters too

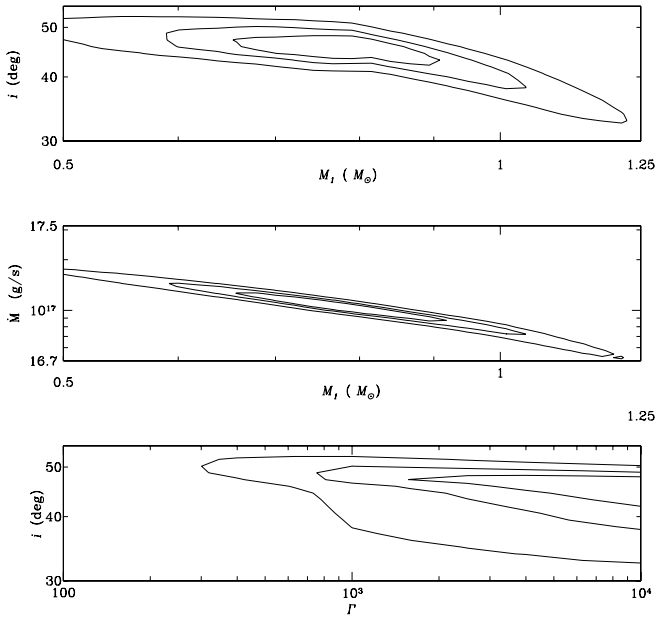

Fig. 11. Confidence contours from χ^2-fitting for AM CVn with $R_{out} = R_{st}$. Inner to outer: 99%, 90% and 66% confidence level.

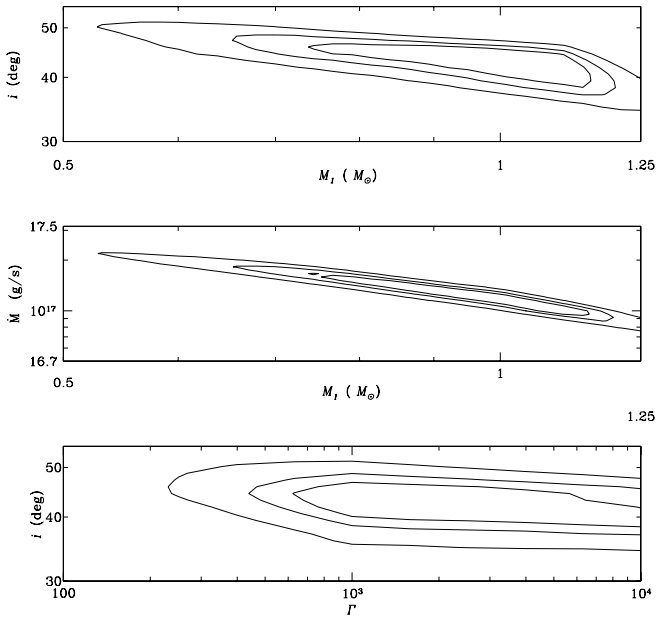

Fig. 12. Confidence contours from χ^2-fitting for AM CVn with $R_{out} = R_{L1}$. Inner to outer: 99%, 90% and 66% confidence level.

– are dependent on more accurate estimation of R_{out}, including possible orbital-eccentricity effects. Nevertheless, we believe that parameter estimates based on R_{st} and R_{L1} give reasonable lower and upper limits respectively. Another interaction shown in the results is a correlation between $\dot{M}$ and M_1, evident from the sloping $M_1 - \dot{M}$ confidence contours. Eq. (1) shows that this correlation arises because, for fixed T_{eff} at disc radius R, an increase in M_1 requires a corresponding decrease in $\dot{M}$.

We choose $R_{out} = R_{L1}$ to present final fitting results. Fig. 13a shows that part of the observed spectrum where χ^2-minimisation is applied, on which is superimposed the best-fit model spectrum when $R_{out} = R_{L1}$. Fig. 13b shows the same best-fit model spectrum superimposed on the full observed spectrum. Using (20), these results indicate that the distance d of AM CVn from the Earth lies in the interval 338–495pc. Mean colours B-V and U-B from observed and predicted data for AM CVn are compared in the upper part of Table 2: despite a possible bias caused by the $3550 \leq \lambda \leq 6150$ bandpass for observed data, there is less than 1.5% difference between corresponding values.

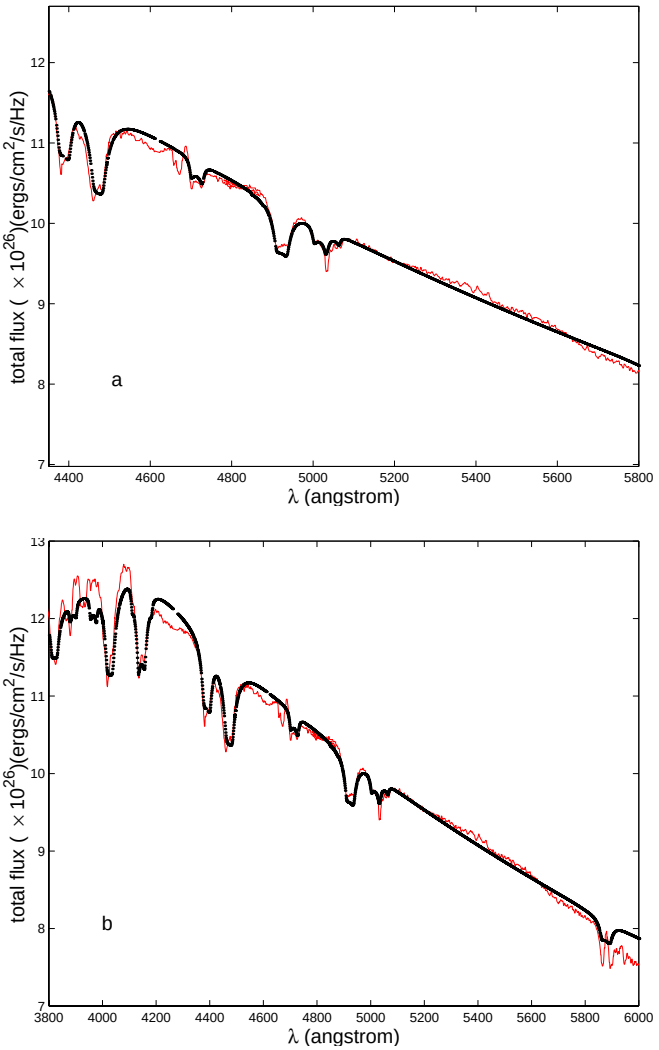

Fig. 13a and b. Observed spectrum of AM CVn (thin line) superimposed on the best-fit spectrum (thick line) with $R_{out} = R_{L1}$. Panel **a** shows that part of the spectrum where χ^2-minimisation is applied. Panel **b** shows the full spectrum.

4.4. Models of best fit for CR Boo

In Figs. 14 and 15 we present confidence contours from the χ^2-fitting for CR Boo with $R_{out} = R_{st}$ and R_{L1}. Best-fit parameters, with one standard deviation error estimates, are:

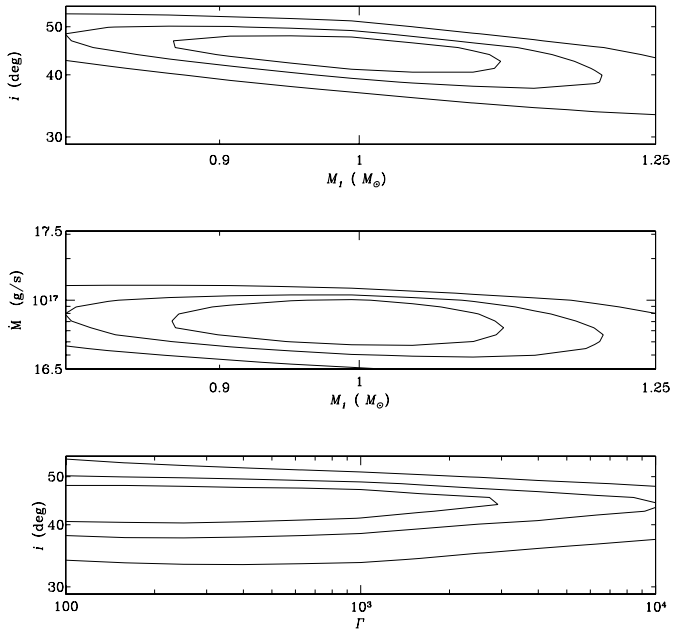

Fig. 14. Confidence contours from χ^2-fitting for CR Boo with $R_{out} = R_{st}$. Inner to outer: 99%, 90% and 66% confidence level.

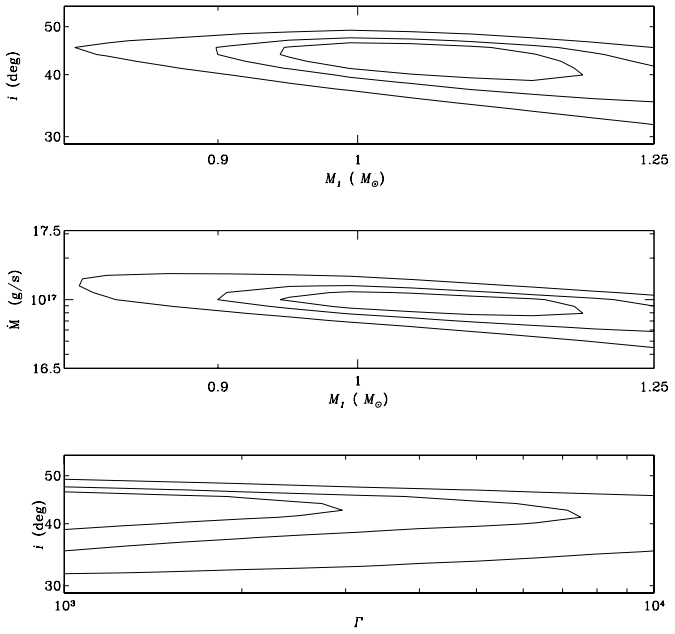

Fig. 15. Confidence contours from χ^2-fitting for CR Boo with $R_{out} = R_{L1}$. Inner to outer: 99%, 90% and 66% confidence level.

Table 2. Mean colours for AM CVn and CR Boo

mean colour	observed	predicted
AM CVn		
B-V	-0.074	-0.073
U-B	-0.955	-0.966
CR Boo		
B-V	-0.050	-0.072
U-B	-0.972	-0.966

- $R_{out} = R_{st}$ gives $M_1 = 0.98 M_\odot \pm 0.1$, $\log \dot{M}(\mathrm{gs}^{-1}) = 16.8 \pm 0.3$ and $i = 44.6^o \pm 3.2$; while
- $R_{out} = R_{L1}$ gives $M_1 = 1.0 M_\odot \pm 0.1$, $\log \dot{M}(\mathrm{gs}^{-1}) = 17.0 \pm 0.2$ and $i = 43.0^o \pm 3.2$.

Averaged values are $M_1 = 0.99 M_\odot$, $\log \dot{M}(\mathrm{gs}^{-1}) = 16.9$ and $i = 43.8^o$. Again the value for M_1 is near the $0.65 M_\odot$ peak value of the distribution of primary masses predicted for AM CVn systems in TY96.

Unfortunately it is not possible to find a lower limit for Γ, as indicated by the open $i - \Gamma$ confidence contours. This is because adverse signal-to-noise levels in the CR Boo data make it difficult to accurately measure H_β line widths. And this inherent data limitation means that the computing-time cost of extending the Γ grid below 10^2 is not warranted. In any case, additional fitting based on metal lines may be needed for more accurate constraints on Γ, which requires extension of the model to include metal opacities.

Once again, difference in fit between the two cases are not great. Indeed, in comparison with the AM CVn fitting, while similar interaction effects between CR Boo disc parameters are seen, they are not nearly as significant. Using $R_{out} = R_{L1}$ to present final fitting results, Fig. 16a shows that part of the observed spectrum where χ^2-minimisation is applied, on which is superimposed the best-fit model spectrum when $R_{out} = R_{L1}$. Fig. 16b shows the same best-fit model spectrum superimposed on the full observed spectrum. Note the crude fitting of the continuum around the Fe/Mg-blend feature near $\lambda 5170$, which – as mentioned earlier – is not within the spectral interval used for χ^2-minimisation.

Using (20), these results indicate that the distance d of CR Boo from the Earth lies in the interval 191–221pc. Mean colours B-V and U-B from observed and predicted data for CR Boo are compared in the lower part of Table 2: note that there is a possible bias caused by the $3450 \leq \lambda \leq 6450$ bandpass for observed data. The difference between predicted and observed mean colours is less than 1% for U-B but, probably because the Fe/Mg-blend feature is lacking in our model, is about 44% for B-V. Nevertheless, our estimates of mean colours for CR Boo are well within those of Wood et al. (1987). Furthermore, our results are consistent with observational data (Warner 1995) suggesting that mean colours for CR Boo in a high state are similar to those of AM CVn.

5. Discussion and conclusions

It is widely believed (Warner 1995) that AM CVn systems are cataclysmic variables at a late evolutionary stage. A plausible scenario (TY96) has them originating as high-mass wide binaries which evolve through two common envelope stages, leaving components which are remnant cores from evolved stars. The present accretor's progenitor would have been initially the more massive, typically leaving a C-O white dwarf after ejection of the first common envelope. The less massive – and hence less evolved – progenitor of the present donor enters the second com-

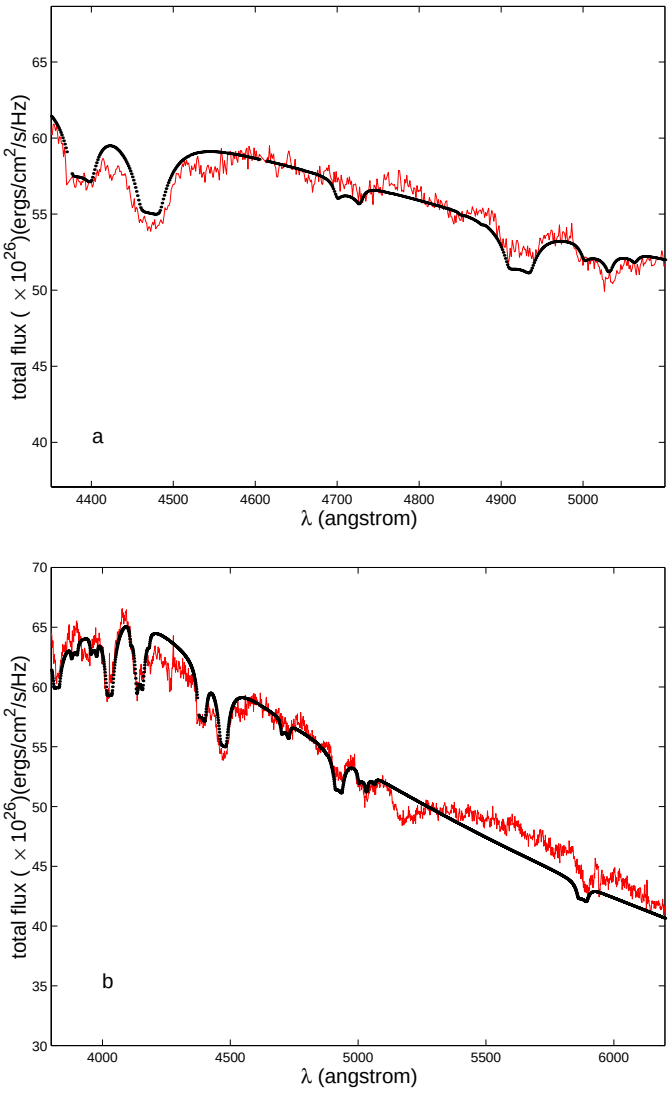

Fig. 16a and b. Observed spectrum of CR Boo (thin line) superimposed on the best-fit spectrum (thick line) with $R_{out} = R_{L1}$. Panel **a** shows that part of the spectrum where χ^2-minimisation is applied. Panel **b** shows the full spectrum.

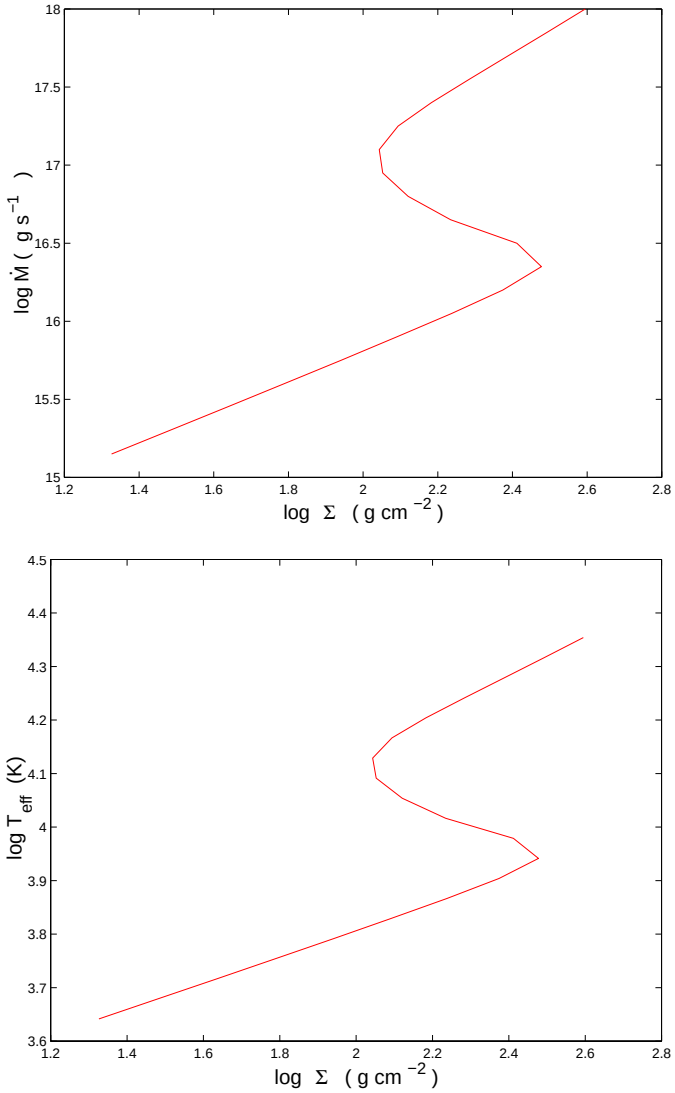

Fig. 17. S-curves for the best-fit AM CVn model with $R_{out} = 8.7 \times 10^9$ cm, $M_1 = 0.84 M_\odot$ and $\log \Gamma = 3$.

mon envelope stage with a helium-rich core. They emerge from the second common envelope stage as a short-period binary and, when orbital angular momentum losses from gravitational radiation bring them close enough for the present donor to experience Roche lobe overflow, mass transfer at rate $\dot{M}$ through a helium-rich accretion disc commences.

During this latter quasi-stable mass-transfer phase, assuming mass conservation but orbital angular momentum losses from gravitational radiation, the donor's mean mass-loss rate $\dot{M}_2$ is related to the orbital period P_{orb} by (Warner 1995)

$$\dot{M}_2 = 8 \times 10^{17} \frac{q^2}{(1+q)^{1/3}} \left(\frac{5}{6} + \frac{\xi_{ad}}{2} - q \right)^{-1} \times \left(\frac{M_1}{M_\odot} \right)^{8/3} \left(\frac{P_{orb}}{1\mathrm{hr}} \right)^{-8/3} \mathrm{gs}^{-1} \quad (34)$$

where, for entropy S

$$\xi_{ad} = \left. \frac{\partial \ln R_2}{\partial \ln M_2} \right|_S \quad (35)$$

is the donor's adiabatic radius-mass coefficient. If the accretion disc is in a *stable* thermal regime then we expect $\dot{M}_2 \approx \dot{M}$ but if, on the other hand, it is in an *unstable* regime then we expect

- $\dot{M}_2 > \dot{M}$ if the system is in a low state, and
- $\dot{M}_2 < \dot{M}$ if it is in a high state.

We now consider whether our results are consistent with this general picture and, in particular whether the results

- support the thermal disc-instability explanation of the brightness variations observed in CR Boo but not in AM CVn, and
- throw any light on the level of degeneracy in the helium-rich binary component.

5.1. Thermal stability of the best-fit AM CVn disc

For the purposes of studying disc stability we take the average of relevant best-fit parameters from Sect. 4.3 for the AM CVn model. The mean value $M_1 = 0.84M_\odot$ and we know that $P_{orb} = 1028.7$s, so with the fully-degenerate donor mass $M_2 = 0.046M_\odot$ and $\xi_{ad} = -1/3$ from Sect. 3.3 we find $\log \dot{M}_2(\mathrm{gs}^{-1}) = 16.8$. As this is approximately the same as the average disc mass-transfer rate $\log \dot{M}(\mathrm{gs}^{-1}) = 17.0$, our results are consistent with the observed stable behaviour of AM CVn.

If we assume a semi-degenerate donor mass $M_2 = 0.092M_\odot$ with $\xi_{ad} = -0.19$ then $\log \dot{M}_2(\mathrm{gs}^{-1}) = 17.4$. As this is a factor of 2.5 greater than the average disc mass-transfer rate from modelling, a semi-degenerate donor seems inconsistent with the observed stable behaviour of AM CVn. Further supportive evidence for a fully-degenerate donor in AM CVn comes from the detectable upper limit $50\,\mathrm{km\,s}^{-1}$ on K_1 noted by PHS. Using averaged best-fit values for AM CVn parameters, we find that $K_1 = 32\,\mathrm{km\,s}^{-1}$ with the fully-degenerate donor and $62\,\mathrm{km\,s}^{-1}$ with the semi-degenerate one: so a fully-degenerate donor seems more plausible on these grounds too.

If the above arguments about thermal stability of the best-fit AM CVn model hold, then we should be able to find an R_{out} within the allowable $R_{st} \le R_{out} \le R_{L1}$ interval for which the whole best-fit disc is thermally stable. In fact using the average best-fit parameters, $R_{out} = 8.7 \times 10^9$cm – which is within the $7.1 \times 10^9 \le R_{out}(\mathrm{cm}) \le 9.2 \times 10^9$ allowable range – generates an S-curve which places AM CVn just on the stable branch. This is shown in Fig. 17, where it is clear that the upper turning-point occurs at $\log \dot{M}(\mathrm{gs}^{-1}) = 17.0$, and any part of the disc inside this radius will also be stable at that mass-transfer rate. Hence our best-fit parameters are able to give disc models for AM CVn that are thermally stable, which is in accord with observations.

5.2. Thermal stability of the best-fit CR Boo disc

For CR Boo, the mean value $M_1 = 0.99M_\odot$ and we know that $P_{orb} = 1471$s, so with the fully-degenerate donor mass $M_2 = 0.032M_\odot$ and $\xi_{ad} = -1/3$ we find $\log \dot{M}_2(\mathrm{gs}^{-1}) = 16.1$. As this is considerably less than the average disc mass-transfer rate $\log \dot{M}(\mathrm{gs}^{-1}) = 16.9$, our results are consistent with CR Boo being in the instability regime but in a high state.

If we assume a semi-degenerate donor mass $M_2 = 0.058M_\odot$ with $\xi_{ad} = -0.19$, then $\log \dot{M}_2(\mathrm{gs}^{-1}) = 16.7$. As this is also considerably less than the average disc mass-transfer rate from modelling, a semi-degenerate donor is also consistent with the observed unstable behaviour of CR Boo. The predicted value of K_1 for CR Boo using averaged best-fit parameters are $18\,\mathrm{km\,s}^{-1}$ for a fully-degenerate donor and $32\,\mathrm{km\,s}^{-1}$ for the fully-degenerate donor. Both values are too small to be detectable at present, so no conclusion may be drawn from them about the nature of the secondary in CR Boo.

If the best-fit CR Boo model is in the instability regime as suggested above, then we should be able to find a best-fit disc satisfying $R_{st} \le R_{out} \le R_{L1}$, within which there is a region where $\dot{M}_2$ lies on the unstable branch of the S-curve but $\dot{M}$ lies on the hot branch. We find that $R = 7.0 \times 10^9$cm – which is within the $9.4 \times 10^9 \le R_{out}(\mathrm{cm}) \le 1.3 \times 10^{10}$ allowable range – generates an S-curve which does just this. This is shown in Fig. 18, where the upper turning-point occurs at about $\log \dot{M}(\mathrm{gs}^{-1}) = 16.9$ and $\log \dot{M}_2(\mathrm{gs}^{-1})$ is on the unstable branch. Any part of the disc inside this radius will also be unstable at the average CR Boo mass-transfer rate as is also shown in Fig. 18 for $R = 5 \times 10^9$ cm. Hence our best-fit parameters are able to give disc models for CR Boo that are thermally unstable, which is in accord with observations.

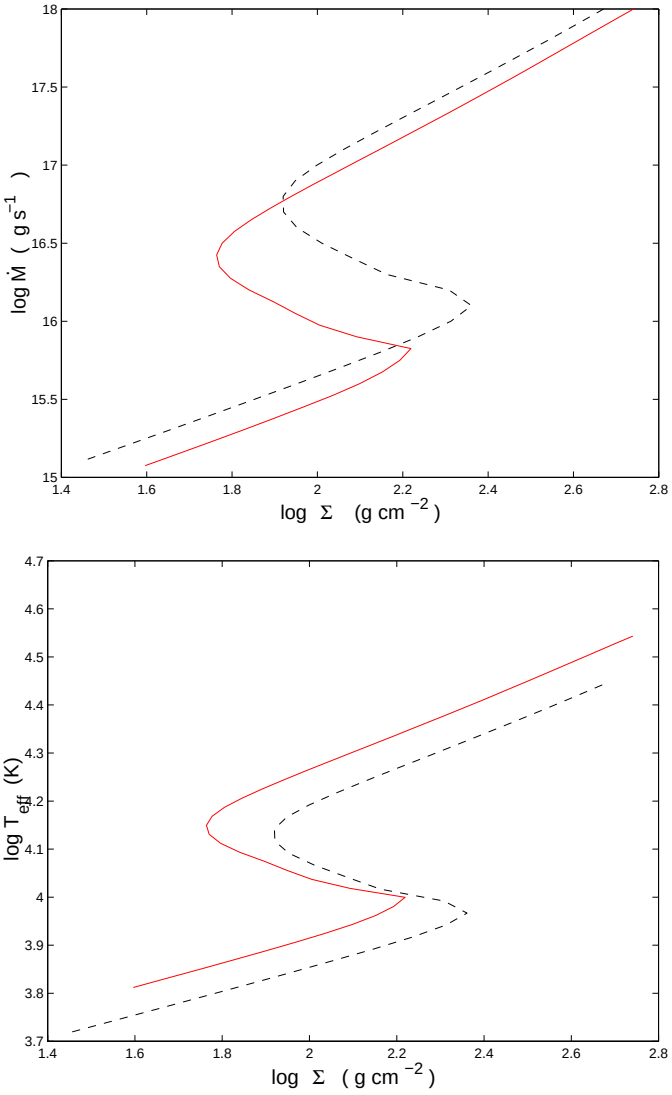

Fig. 18. S-curves for the best-fit CR Boo model with $M_1 = 0.99M_\odot$ and $\log \Gamma = 3$. Dashed line: $R = 7 \times 10^9$ cm. Solid line: $R = 5 \times 10^9$ cm.

However, S-curves also depend on Γ which, in our fitting, has a large error range: Fig. 19 shows CR Boo S-curves for $R = 1.0 \times 10^{10}$ cm with $\log \Gamma = 2$, 3 and 4. It is clear that a higher hydrogen content can reduce the effective temperature of the instability region. The kink in the $\log \Gamma = 2$ curve shows that the helium instability strip – evident in the $\log \Gamma = 4$ case

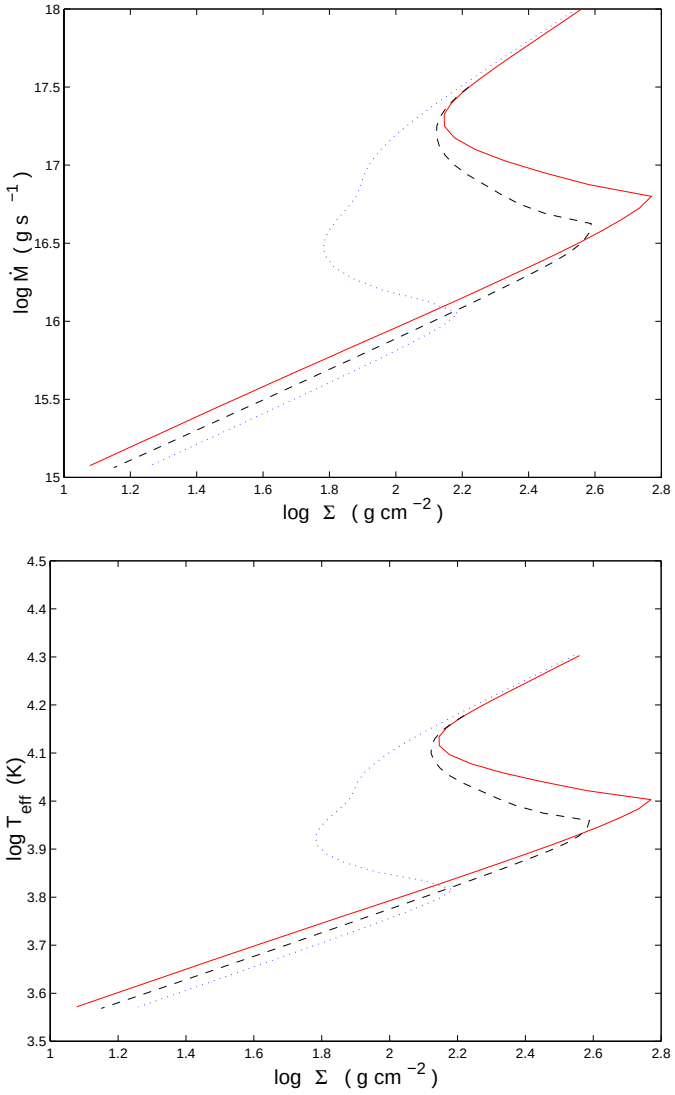

Fig. 19. S-curves for the best-fit CR Boo model with $M_1 = 0.99M_\odot$ at $R = 1.0 \times 10^{10}$ cm. Dotted line: $\log \Gamma = 2$. Dashed line: $\log \Gamma = 3$, Solid line: $\log \Gamma = 4$.

– has almost disappeared. Hence the nature of the instability region does not only depend on R, but also on Γ.

5.3. The nature of the secondary

We have seen from above there is some evidence that the donor in AM CVn is fully-degenerate, although there is no such evidence for CR Boo. A possible source of independent information on the mass – and therefore degeneracy status – of the donor in AM CVn systems comes from tidal resonance models of the superhump phenomenon. These models predict a beat period P_b arising between superhump period P_s and orbital period P_{orb}, where

$$\frac{1}{P_b} = \frac{1}{P_{orb}} - \frac{1}{P_s}. \tag{36}$$

There is strong evidence for the tidal resonance model, both from photometric and spectroscopic analysis, in hydrogen-rich cataclysmic variables with superhumps such as OY Car, HT Cas and Z Cha (PHS, Warner 1995).

Furthermore, if we identify the 1051s periodicity seen in AM CVn with a superhump period, then applying (36) yields $P_b = 13.36$hrs for the AM CVn orbital period $P_{orb} = 1028.7$s. And similarly the hypothesised 1490s superhump period in CR Boo gives $P_b = 32.0$ hrs. Now (Warner 1995) the tidal resonance model for superhumps leads to the relationship

$$\frac{P_b}{P_{orb}} = \frac{3.73(1+q)}{q} \tag{37}$$

for low mass ratios q. Hence, for AM CVn we find $q = 0.087$, which, using our average best-fit estimate $M_1 = 0.84M_\odot$, results in $M_2 = 0.07M_\odot$, between our estimates of fully and semi-degenerate secondary masses. Similarly for CR Boo $q = 0.05$ which, for $M_1 = 0.99M_\odot$, gives $M_2 = 0.05M_\odot$ – also between fully and semi-degenerate estimates.

Finally, we stress while the quoted errors are formal errors of the fitting procedure, they may be an underestimate of the true systematic errors when our model approximations are relaxed.

5.4. Conclusions

We conclude that a simple helium-rich disc model may be fitted to observed spectra of AM CVn and CR Boo. Resulting mean accretor masses are close to, but somewhat higher than, the 0.7–$0.8M_\odot$ range predicted by present population synthesis studies, while modelled helium-to-hydrogen number density ratios are consistent with a helium-degenerate donor surrounded by a helium-rich envelope.

Predicted disc mass-transfer rates of about 10^{17}gs^{-1} may place the systems in the region of potential disc instability. In fact, S-curves calculated for the best-fit models are consistent with a thermally-stable disc in AM CVn, and a thermally unstable disc in CR Boo.

Acknowledgements. We thank Dr Stephen Roberts for help with computational aspect of this paper, and Dr Stéphane Vennes for valuable discussions and for providing line and continuum opacity routines. Professor Joseph Patterson kindly supplied spectral data on CR Boo. We are also grateful to both Professor Ronald Webbink and Michael Burgess for their helpful comments and advice.

References

Adam J., Störzer H., Shaviv G., Wehrse R., 1988, A&A 193, L1
Brenan K.E., Campbell S.L., Petzold L.R., 1989, Numerical Solution of Initial-Value Problems in Differential-Algebraic Equations. Elsevier, New York
Burbidge G., Burbidge M., Hoyle F., 1967, ApJ 147, 121
Burbidge E.M., Strittmatter P.A., 1971, ApJ 170, L39
Eggleton P.P., 1983, ApJ 268, 368
Faulkner J., Flannery B.P., Warner B., 1972, ApJ 175, L79
Frank J., King A.R., Raine D., 1992, Accretion Power in Astrophysics. Cambridge Univ. Press, Cambridge
Greenstein J.L., Mathews M.S., 1957, ApJ 126, 14
Harvey D.A., Skillman D.R., Kemp J., et al., 1998, ApJ 493, L105

Howell S.B., Szkody P., Kreidel T.J., Dobrzycka D., 1991, PASP 103, 300
Humason M.L., Zwicky F., 1947, ApJ 105, 85
Malmquist K.G., 1936, Stockholms Observatoriums Annaler Vol. 12, 7, 130
Nather R.E., 1985, In: Eggleton P.P., Pringle J.E. (eds.) NATO ASI Ser. C Vol.150, Interacting Binaries. Reidel, Dordrecht, p. 349
Nauenberg M., 1972, ApJ 175, 417
O'Donoghue D., Menzies J., Hill P.W., 1987, MNRAS 227, 295
O'Donoghue D., Kilkenny D., Chen A., et al., 1994, MNRAS 271, 910
Osaki Y., 1996, PASP 108, 390
Paczyński B., 1971, ARA&A 9, 183
Paczyński B., 1977, ApJ 216, 822
Patterson J., Sterner E., Halpern J., Raymond J.C., 1992, ApJ 384, 234
Patterson J., Halpern J., Shambrok A., 1993, ApJ 419, 803
Patterson J., Kemp J., Shambrook A., Thomas E., 1997, PASP 103, 1100
Savonije G.J., de Kool M,. Van den Heuvel E.P.J., 1986, A&A 155, 51
Shakura N.I., Sunyaev R., 1973, A&A 24, 337
Shaviv G., Wehrse R., 1986, A&A 159, L5
Smak J., 1967, Acta Astron. 17, 255
Tutukov A., Yungelson L., 1996, MNRAS 280, 1035
Wade R.A., 1984, MNRAS 208, 381
Wampler E.J., 1967, ApJ 149, L101
Warner B., 1972, MNRAS 159, 315
Warner B., Robinson E.L., 1972, MNRAS 159, 101
Warner B., 1995, Cataclysmic Variable Stars. Cambridge Univ. Press, Cambridge
Wehrse R., Baschek B., Shaviv G., 1994, In: Shafter A.W. (ed.) ASP Conf. Ser. Vol. 56, Interacting Binary Stars. Brigham Young Univ., Provo, p. 35
Wood M.A., Winget D.E., Nather R.E., Hessman F.V., 1987, ApJ 313, 757